It has been pointed out (*26*) that this scenario is particularly appealing, because other nonstellar injection models suffer the disadvantage of both having to account for the fractionation through other means and facing the prospect that the remarkable similarity between the cosmic-ray source composition and the composition of solar energetic particles is purely accidental. However, this hypothesis is based entirely on extrapolation of the solar case, because before now it has not been possible to determine the abundances of elements in the coronae of other stars. Our failure to detect a similar FIP effect in the corona of Procyon provides evidence that the FIP effect is not a ubiquitous signature of late-type stellar coronae.

REFERENCES AND NOTES

1. S. R. Pottasch, *Astrophys J.* **137**, 945 (1963).
2. A. Mogro-Campero and J. A. Simpson, *ibid.* **171**, L5 (1972).
3. A. B. C. Walker, H. R. Rugge, K. Weiss, *ibid.* **194**, 471 (1974).
4. H. R. Rugge and A. B. C. Walker, *ibid.* **203**, L139 (1976).
5. J. H. Parkinson, *Astron. Astrophys.* **57**, 185 (1977).
6. J.-P. Meyer, *Astrophys. J. Suppl. Ser.* **57**, 172 (1985).
7. M. Cassé and P. Goret, *Astrophys. J.* **221**, 703 (1978).
8. U. Feldman, *Phys. Scr.* **46**, 202 (1992).
9. S. Bowyer and R. F. Malina, in *Extreme Ultraviolet Astronomy*, R. F. Malina and S. Bowyer, Eds. (Pergamon, New York, 1991), p. 94.
10. R. Griffin, *Mon. Not. R. Astron. Soc.* **155**, 139 (1971).
11. J. Tomkin and D. L. Lambert, *Astrophys. J.* **223**, 937 (1978).
12. K. Kato and K. Sadakane, *Astron. Astrophys.* **167**, 111 (1986).
13. M. Steffen, *Astron. Astrophys. Suppl. Ser.* **59**, 403 (1985).
14. B. Edvardsson *et al.*, *Astron. Astrophys.* **275**, 101 (1993).
15. J. H. M. M. Schmitt *et al.*, *Astrophys. J.* **290**, 307 (1985).
16. B. Haisch, J. J. Drake, J. H. M. M. Schmitt, *ibid.* **421**, L39 (1994).
17. K. G. Widing and U. Feldman, *ibid.* **334**, 1046 (1989).
18. J. H. M. M. Schmitt, B. M. Haisch, J. J. Drake, *Science* **265**, 1420 (1994).
19. P. L. Dufton, personal communication; D. R. Flower and H. Nussbaumer, *Astron. Astrophys.* **31**, 353 (1974); B. C. Fawcett and H. E. Mason, *At. Data Nucl. Data Tables* **43**, 245 (1989); H. E. Mason and A. K. Bhatia, *Mon. Not. R. Astron. Soc.* **184**, 423 (1978); D. F. Flower and H. Nussbaumer, *Astron. Astrophys.* **42**, 265 (1975).
20. R. J. Thomas and W. M. Neupert, *Astrophys. J. Suppl. Ser.* **91**, 461 (1994).
21. M. Malinovsky and L. Heroux, *Astrophys. J.* **181**, 1009 (1973).
22. J. Murthy *et al.*, *ibid.* **315**, 675 (1987).
23. C. J. Schrijver, *Astron. Astrophys.* **180**, 241 (1987).
24. R. von Steiger and J. Geiss, *ibid.* **225**, 222 (1989).
25. W. I. Axford, E. Leer, K. G. Skandron, *Proc. 15th Int. Cosmic Ray Conf.* **11**, 32 (1977).
26. H. Bloemen, in *Interstellar Processes*, D. J. Hollenbach and H. A. Thronson Jr., Eds. (Reidel, Dordrecht, Netherlands, 1987), p. 143.
27. U. Feldman, J. D. Purcell, B. C. Dohne, *NRL Rep. 90-4100* and *NRL Rep. 91-4100* (Naval Research Laboratory, Washington, DC, 1987).
28. E. Anders and N. Grevesse, *Geochim. Cosmochim. Acta* **53**, 197 (1989).

29. We thank G. Doschek, U. Feldman, K. Strong, and J. Saba for useful discussions and the EUVE Science Team for advice and support. We thank the referees for pertinent comments, which improved the manuscript. J.J.D. was supported by National Aeronautics and Space Administration grant AST91-15090 administered by the Center for Extreme Ultraviolet Astrophysics, University of California.

18 August 1994; accepted 28 December 1994

Conducting Layered Organic-Inorganic Halides Containing ⟨110⟩-Oriented Perovskite Sheets

D. B. Mitzi,* S. Wang, C. A. Feild, C. A. Chess, A. M. Guloy

Single crystals of the layered organic-inorganic perovskites, $[NH_2C(I)=NH_2]_2(CH_3NH_3)_mSn_mI_{3m+2}$, were prepared by an aqueous solution growth technique. In contrast to the recently discovered family, $(C_4H_9NH_3)_2(CH_3NH_3)_{n-1}Sn_nI_{3n+1}$, which consists of ⟨100⟩-terminated perovskite layers, structure determination reveals an unusual structural class with sets of m ⟨110⟩-oriented $CH_3NH_3SnI_3$ perovskite sheets separated by iodoformamidinium cations. Whereas the $m = 2$ compound is semiconducting with a band gap of 0.33 ± 0.05 electron volt, increasing m leads to more metallic character. The ability to control perovskite sheet orientation through the choice of organic cation demonstrates the flexibility provided by organic-inorganic perovskites and adds an important handle for tailoring and understanding lower dimensional transport in layered perovskites.

Recent interest in organic-inorganic multilayer perovskites stems from the flexibility to use organic layers to tailor magnetic (*1*, *2*), optical (*3*, *4*), thermochromic (*5*), or structural (*6*) properties of adjacent nonconducting metal halide perovskite sheets. Typically, these self-assembling structures consist of single ⟨100⟩-terminated perovskite sheets alternating with alkylammonium bilayers, with the alkyl chains extending into the space between layers and van der Waals interactions between chains holding the layers together. More complicated organic cations have also been incorporated, including those with benzene rings and unsaturated hydrocarbon tails (*4*, *7*). The ability to polymerize the organic layer (*7*, *8*) or to study conformational changes within long-chain alkylammonium bilayers (*9*) provides further flexibility and interest.

Recently, a family of conducting layered organic-inorganic perovskites, $(C_4H_9NH_3)_2(CH_3NH_3)_{n-1}Sn_nI_{3n+1}$ (n = 1 to 5), was found (*10*) in which n ⟨100⟩-terminated $CH_3NH_3SnI_3$ perovskite sheets alternate with butylammonium bilayers. These conducting non–oxide-layered perovskites share many of the structural features of the cuprate superconductors and other conducting layered-oxide perovskites (which also consist of ⟨100⟩ perovskite sheets). In addition, these systems are natural (self-assembling) analogs to semiconductor quantum-well multilayers, with the perovskite layers acting as wells and the longer-chain alkyl layers forming barrier layers. Observation of enhanced exciton binding energies in both the lead(II) and tin(II) analogs of these layered perovskites highlight the two-dimensional nature and the effect of dielectric modulation (*3*, *11*).

In this report, we discuss the synthesis, structure, and transport properties of a class of conducting layered halides, $[NH_2C(I)=NH_2]_2(CH_3NH_3)_mSn_mI_{3m+2}$ (m = 2 to 4), that consists of m $CH_3NH_3SnI_3$ perovskite layers terminating on a ⟨110⟩ crystallographic plane, rather than on the usual ⟨100⟩ plane. This structure appears to be stabilized by the interposed layers of iodoformamidinium cations, which orient along the channels provided by the ⟨110⟩ perovskite surfaces. The ability to form either ⟨100⟩- or ⟨110⟩-terminated perovskite sheets through the choice of organic cation in the initial crystal growth solution (in this case, butylammonium versus iodoformamidinium) demonstrates an additional degree of flexibility within the family of organic-inorganic perovskites. Many of the related ⟨100⟩-terminated conducting layered perovskites—including the oxides $(La_{1-x}Sr_x)_{n+1}Mn_nO_{3n+1}$ (*12*), $La_{n+1}Ni_nO_{3n+1}$ (*13*), and $Ba_{n+1}Pb_nO_{3n+1}$ (*14*) as well as the halide $(C_4H_9NH_3)_2(CH_3NH_3)_{n-1}Sn_nI_{3n+1}$ (*10*)—undergo a semiconductor-metal transition with increasing n. We find a similar trend in the ⟨110⟩-terminated layered perovskites.

Crystals of each tin(II)-based layered perovskite were grown in an argon atmosphere by slow cooling from concentrated aqueous hydriodic acid solutions of CH_3NH_2·HI, NH_2CN, and SnI_2 (*15*). The chemistry of cyanamide in this synthesis is in itself unusual. Although anhydrous reaction between nitriles (RCN) and hydrogen halides (HX) generally results in the nucleophilic attack of X^- on the nitrile triple bond (resulting in an

D. B. Mitzi, C. A. Feild, C. A. Chess, IBM T. J. Watson Research Center, Post Office Box 218, Yorktown Heights, NY 10598, USA.
S. Wang and A. M. Guloy, Department of Chemistry and Texas Center for Superconductivity, University of Houston, Houston, TX 77204–5641, USA.

*To whom correspondence should be addressed.

imidyl halide), in aqueous acid solutions, cyanamide generally hydrolyzes to give urea (*16*). Kilpatrick (*17*) has demonstrated that the rate of hydrolysis in aqueous hydrochloric and hydrobromic acids increases to a maximum with increasing acid concentration and thereafter drops off as a result of the formation of competing less-hydrolyzable species. It is likely that our use of the stronger concentrated aqueous hydriodic acid effectively avoids the hydrolysis of cyanamide through a similar process, with the formation of the iodoformamidinium cation, which has greater hydrolysis resistance.

Infrared (IR) transmission spectroscopy of cleaved $m = 2$ single crystals confirms that these solid-state structures contain the iodoformamidinium cation. A strong band at 1652 cm^{-1} is characteristic of the amidine (N–C=N) stretching vibration (*18*). A second strong band is observed at 1712 cm^{-1}. Sumarokova *et al.* (*19*) assign bands at 1710 and 1665 cm^{-1} in diacetonitrile hydrogen chloride tin(IV) chloride to C=N stretching modes. A strong band at 604 cm^{-1} corresponds to the C–I stretch, and bands at 3327, 3263, and 3180 cm^{-1} correspond to the N–H_2 asymmetric and the N–H and N–H_2 symmetric stretches, respectively. In addition, two bands are observed at 1473 cm^{-1} (C–NH_2 deformation mode) and 1389 cm^{-1} (C–N stretch). Bands characteristic of hydrogen iodide and nitrile (C≡N) moieties, from the starting material, would be expected from 2100 to 2400 cm^{-1} and are not observed, and absorptions attributed to urea, especially the carbonyl expected between 1650 and 1500 cm^{-1} (*20*), are also not observed.

The organic-inorganic multilayer structure (Fig. 1 and Table 1) of $[NH_2C(I)=NH_2]_2(CH_3NH_3)_2Sn_2I_8$ ($m = 2$), as derived from a single-crystal structure refinement, has a monoclinic unit cell with a = 6.2649(4) Å, b = 8.6624(5) Å, c = 14.787(2) Å, and β = 92.960(8)° (numbers in parentheses are standard errors in the last digit). The perovskite sheets are derived from the three-dimensional perovskite structure of $CH_3NH_3SnI_3$, which consists of an infinite network of corner-sharing SnI_6 octahedra, by cutting two-layer-thick perovskite slabs terminating on ⟨110⟩ planes. Similar ⟨110⟩-terminated perovskite sheets also appear in a series of nonconducting inorganic oxides with general formula $A_mM_mO_{3m+2}$ (where A = Ca, Na/Ca or La, La/Ca; and M = Nb or Ti) (*21*) and in the fluorides $BaMF_4$ (where M = Ni, Co, Mn, or Fe) (*22*).

The tin(II) halide perovskites are unusual in that the tin(II) lone pair is stereochemically inactive, enabling tin(II) to achieve an uncharacteristic regular octahedral coordination (trigonal or square pyramidal coordination is more typical), presumably because the tin 5*s* nonbonding states are delocalized into a conduction band (*23*). Within the perovskite slabs (Fig. 2) of $[NH_2C(I)=NH_2]_2(CH_3NH_3)_2Sn_2I_8$, the tin(II) atoms sit in a slightly distorted octahedral coordination with I–Sn–I angles ranging from 85.67(5)° to 92.82(6)° and Sn–I bond distances ranging from 3.094(2) to 3.185(1) Å, where the shortest bonds are to the outer terminal iodines, I(3), and the longest are to the central layer of iodines, I(1). These values can be compared with the 90° I–Sn–I bond angles and six equal 3.12 Å Sn–I bonds in cubic (at room temperature) $CH_3NH_3SnI_3$. The Sn–I(2)–Sn angle of 173.3(1)° indicates a slight corrugation of the tin(II) iodide perovskite sheets along the a axis. The $CH_3NH_3^+$ cations are located on the A sites of the ABX_3 perovskite slabs, coordinated by 11 iodines from within the perovskite slabs and one iodine from the nearest iodoformamidinium cation, thereby yielding the same overall coordination as in the cubic perovskite.

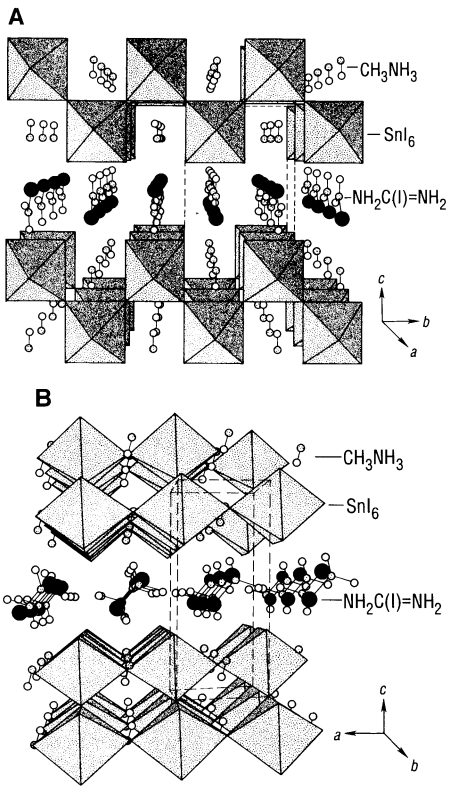

Fig. 1. Two schematic views of the $[NH_2C(I)=NH_2]_2(CH_3NH_3)_2Sn_2I_8$ ($m = 2$) crystal structure, along the (**A**) ⟨100⟩ and (**B**) ⟨010⟩ directions, highlighting the ⟨110⟩ orientation of the $CH_3NH_3SnI_3$ perovskite sheets. The SnI_6 octahedra are shown in a polyhedral representation with the iodine atoms removed for clarity.

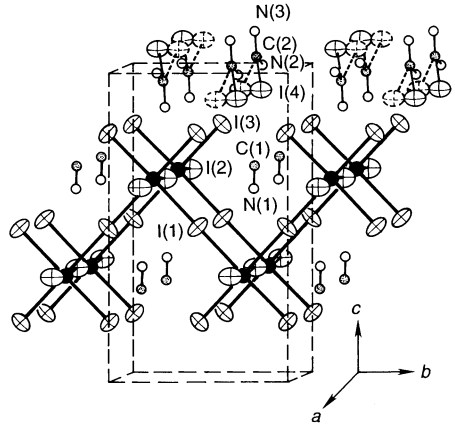

Fig. 2. Detailed structure of the Sn–I perovskite layer showing atom labeling and anisotropic thermal ellipsoids. A split position for I(4) with ½ occupancy indicates disordering of the iodoformamidinium cation.

Table 1. Crystallographic data for $[NH_2C(I)=NH_2]_2(CH_3NH_3)_2Sn_2I_8$. The space group $P2_1/m$ was selected in agreement with systematic absences and intensity distribution. Data were collected at room temperature in the ω-2θ scan mode up to 2θ = 48°, using an Enraf-Nonius CAD4 single-crystal diffractometer and graphite monochromatized MoKα radiation. The θ-dependent absorption correction, based on multiple psi-scans, was applied to all intensity data. Direct methods were used to determine the Sn and I heavy-atom positions, and subsequent refinement and Fourier synthesis steps located the lighter elements (C and N). Numbers in parentheses are statistical errors of the last significant digit (when absent, the parameter was held fixed). Final least squares refinement resulted in refinement parameters R_f/R_w = 0.047/0.051 [10 atoms, 52 parameters, 899 independent reflections with intensities $I \geq 3\sigma(I)$]. a = 6.2649(4) Å, b = 8.6624(5) Å, c = 14.787(2) Å; β = 92.960(8)°; and $Z = 1$.

Atom	Position*	x	y	z	B_{iso} (Å²)†
Sn	2e	0.0156(3)	¼	0.6582(1)	3.5(1)
I1	2c	0	½	½	7.0(1)
I2	2e	0.5207(3)	¼	0.6457(2)	6.7(1)
I3	4f	0.0299(2)	0.4997(2)	0.8080(1)	5.7(1)
I4‡	4f	0.6330(4)	0.6918(4)	0.9379(2)	5.6(2)
N1	2e	0.44(1)	¼	0.378(5)	20 (3)
N2	2e	0.203(5)	¾	0.009(2)	7.7(8)
N3	2e	0.473(6)	¾	0.115(2)	8.5(9)
C1	2e	0.55(1)	¼	0.330(6)	16 (3)
C2	2e	0.416(5)	¾	0.029(2)	5.2(7)

*Multiplicity and Wyckoff letter. †B_{iso} is the mean of the principal axes of the thermal ellipsoid. ‡Occupancy = ½ as a result of orientational disorder.

The $m = 2$ structure is distinct from the insulating $BaZnF_4$ (or equivalently $Ba_2Zn_2F_8$) structure in that the divalent Ba^{2+} cation is replaced by the monovalent $CH_3NH_3^+$ cation. To maintain charge neutrality, an additional monovalent cation needs to be incorporated into the structure, thereby forming the distinct organic layer of this unusual multilayer structure. The organic iodoformamidinium cations are therefore an integral part of the crystal structure and are not simply an intercalated species. The refined bond angles around the iodoformamidinium carbon range from 115° to 123°, consistent with sp^2 hybridization. The refined C(2)–I(4), C(2)–N(2), and C(2)–N(3) distances [2.02(3), 1.35(5), and 1.31(5) Å] are also typical for bonding in this hybridization. Within the solid-state structure, iodoformamidinium cations form nominal "chains" of $NH_2C(I)=NH_2^+$ along the a axis with the I(4) atoms of this cation directed toward and coordinating the nearest $CH_3NH_3^+$ cations in the perovskite sheet. The N(3) atoms orient toward the nearest I(3) atom of the perovskite slabs, whereas N(2) atoms are directed at the I(4) of the neighboring colinear organic cation. Hence, adjacent chains within the layer are oriented anti to each other.

More generally, a family of compounds, $[NH_2C(I)=NH_2]_2(CH_3NH_3)_mSn_mI_{3m+2}$, for $m \geq 1$, are expected. Isolation of the $m = 3$ and 4 members (Fig. 3) confirms this expectation. Lattice parameters for the observed members of $[NH_2C(I)=NH_2]_2(CH_3NH_3)_mSn_mI_{3m+2}$ approximately follow the rule $a = a_p$, $b = \sqrt{2}a_p$, and $c = K + ma_p/\sqrt{2}$, where a_p is defined as the lattice parameter for the cubic perovskite (for $CH_3NH_3SnI_3$, $a_p = 6.240$ Å) and $K \approx 5.98(5)$ Å. The monoclinic angle β is found to decrease with increasing m from 92.96(1)° ($m = 2$) to 91.83(1)° ($m = 4$). Evidence for other m members of this family have also been observed in both single-crystal and powder x-ray data.

Electrical resistivity measurements (Fig. 4) were performed in a displex (closed-cycle refrigeration) system with an airtight cell containing a calibrated four-point probe and a pressed-pellet sample. Given the rather severe chemical reactivity of these materials, ohmic electrical contacts were made with spring-activated pins directly contacting the sample. The $m = 2$ sample is semiconducting with a room-temperature resistivity of ~700 ohm·cm. Fitting the resistivity data to $\rho = A\exp(E_g/2k_BT)$ (Fig. 4, inset), where A is a constant, k_B is Boltzmann's constant, and T is temperature, yields a band gap of $E_g = 0.33(5)$ eV. Increasing the thickness of the perovskite sheets (larger m) dramatically reduces the resistivity and results in a transition to more metal-like transport properties, as has also been observed in the ⟨100⟩-oriented perovskites $(C_4H_9NH_3)_2(CH_3NH_3)_{n-1}Sn_nI_{3n+1}$, which undergo a semiconductor-metal transition with increasing n (*10*). In fact, comparing the resistivity data of the ⟨110⟩ and ⟨100⟩ layered perovskites reveals a consistent exponential drop in low-temperature resistivity with increasing perovskite layer thickness, approximately independent of layer orientation. A semiconductor-metal transition occurs for a perovskite layer thickness on the order of 20 Å, with a corresponding room-temperature resistivity of order 1 ohm·cm at the transition. The resistivity of $CH_3NH_3SnI_3$, which is the end-member compound of both the ⟨110⟩ and ⟨100⟩ families as m (or n) approaches infinity, is also shown for comparison. This cubic (at room temperature) perovskite has recently been shown to be a low–carrier density p-type metal with a well-defined plasma edge in the IR spectrum (*24*).

To better understand the nature of the semiconductor-metal transition in these unusual conducting halides, extended Hückel band structure calculations were performed on the $m = 2$ and $m \rightarrow \infty$ (cubic perovskite) systems, with a basis set consisting of Sn 5*s* and 5*p* and I 5*s* and 5*p* valence orbitals. The metallic character of $CH_3NH_3SnI_3$ results from the large dispersion of the Sn 5*s* band (hybridized with I 5*p*) along the ⟨111⟩ direction of the cubic Brillouin zone, leading to a marginal crossing of the Sn 5*s* and Sn 5*p* bands near the R point ($[\frac{1}{2}, \frac{1}{2}, \frac{1}{2}]2\pi/a$), with the Fermi energy falling roughly between the two bands. Low concentrations of defects or vacancies in the structure are

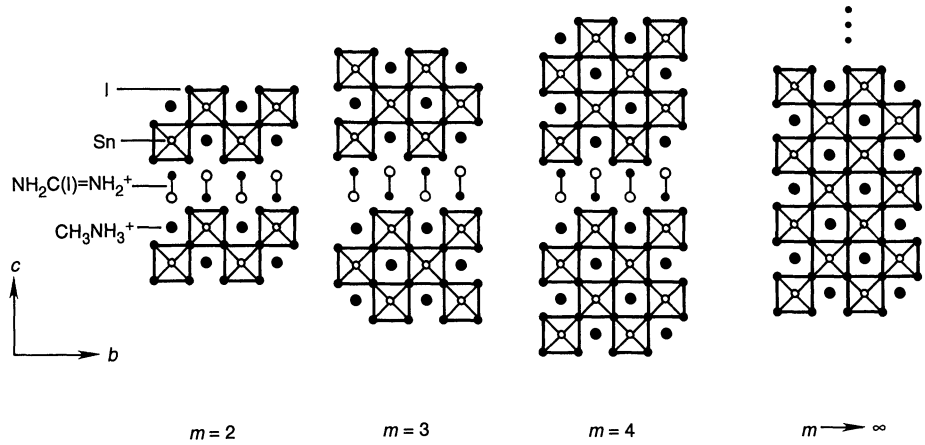

Fig. 3. Schematic representation of the $m = 2$ to 4 and ∞ (cubic perovskite) compounds. The monoclinic lattice constants for $m = 2$, 3, and 4 are $a = 6.2649(4)$ Å, $b = 8.6624(5)$ Å, $c = 14.787(2)$ Å, and $\beta = 92.960(8)°$; $a = 6.2671(3)$ Å, $b = 8.7183(4)$ Å, $c = 38.434(2)$ Å (2 × 19.217), and $\beta = 92.34(2)°$; and $a = 6.2485(7)$ Å, $b = 8.7162(10)$ Å, $c = 23.653(4)$ Å, and $\beta = 91.83(1)°$, respectively. In some crystals examined, weak superstructure reflections indicate a doubling or quadrupling of the basic unit cell along the c axis, perhaps as a result of partial ordering of the iodoformamidinium cations.

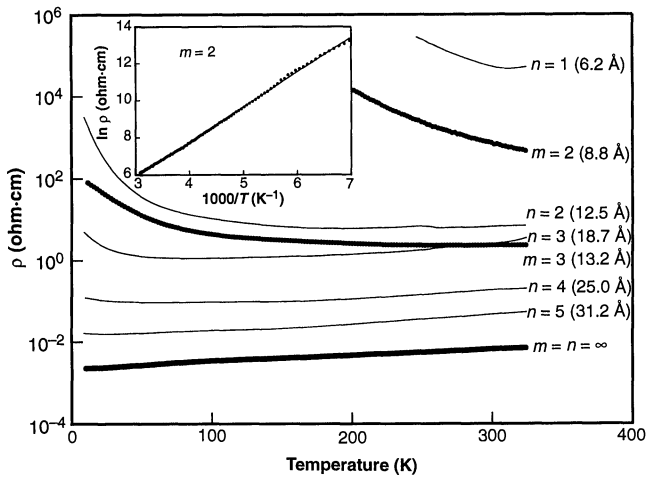

Fig. 4. Resistivity ρ as a function of temperature for pressed-pellet $m = 2$ and 3 samples of $[NH_2C(I)=NH_2]_2(CH_3NH_3)_mSn_mI_{3m+2}$ and the cubic (at room temperature) perovskite $CH_3NH_3SnI_3$ ($m \rightarrow \infty$). For comparison, resistivity data for $(C_4H_9NH_3)_2(CH_3NH_3)_{n-1}Sn_nI_{3n+1}$ are also shown. Distances in parentheses indicate the approximate thicknesses t of the perovskite sheets as calculated from either $t = 6.24m/\sqrt{2}$ or $t = 6.24n$ for the ⟨110⟩ and ⟨100⟩ families, respectively. The inset displays the natural logarithm of resistivity as a function of inverse temperature for $m = 2$. The line drawn through the data points is a least squares fit of the data. Analysis of the slope yields a band gap $E_g = 0.33(5)$ eV.

expected to influence the observed carrier densities (*24*). In going to the $m = 2$ structure, the layering of the perovskite structure results in the formation of terminal Sn–I interactions, which raise the Sn 5*p* antibonding (Sn–I) orbitals to higher energy, as well as reduce the band widths, resulting in a significant band gap (of order 0.5 eV). Increasing m leads to a progressive stabilization of the Sn 5*p* antibonding orbitals and a broadening of the Sn 5*s* and Sn 5*p* band widths, thereby effectively decreasing the band gap and leading to more metallic character. Notably, even for the metallic end-member of the series, $CH_3NH_3SnI_3$, the carrier density, measured by Hall effect (*24*), is only 2×10^{19} holes per cubic centimeter, which is two orders of magnitude smaller than in the superconducting bismuthate or cuprate perovskites. This, combined with the small effective mass ($m^* \approx 0.2$ for $CH_3NH_3SnI_3$), leads to a very small density of states at the Fermi energy, which (at least without doping) is not conducive to superconductivity.

Organic-inorganic multilayer materials, both self-assembling and artificially prepared, are particularly interesting because of the potential for tunability with respect to a given desired property. Artificially prepared organic-inorganic multilayers with interesting optoelectronic properties have, for example, been synthesized with the use of an ionized cluster beam apparatus with multiple ion sources (*25*). Self-assembling organic-inorganic perovskites offer the potential for tunability with, however, much simpler synthetic conditions than for the artificial structures.

Within the family of conducting tin iodide–based layered organic-inorganic perovskites, we have modified the orientation of the conducting perovskite layers through choice of organic cation. As with the ⟨100⟩ family of layered organic-inorganic perovskites, it is expected that the ⟨110⟩ structural family can accommodate a variety of different divalent metal halides, including the first-row transition-metal halides, and lead and cadmium halides, thereby providing additional interesting opportunities for the study of self-assembling multilayer quantum wells, two-dimensional magnetism, and optical, thermochromic, as well as transport properties. A preliminary demonstration of this is our recent synthesis, by the same technique described for the tin(II) compounds, of the lead(II) analog, which has monoclinic lattice parameters similar to those of the $m = 2$ tin compound but with a doubling of the basic unit cell along the b axis: $a = 6.315(3)$ Å, $b = 29.498(6)$ Å, $c = 8.713(1)$ Å, and $\beta = 90.96(3)°$ (*26*).

REFERENCES AND NOTES

1. G. V. Rubenacker, D. N. Haines, J. E. Drumheller, K. Emerson, *J. Magn. Magn. Mater.* **43**, 238 (1984).
2. L. J. de Jongh and A. R. Miedema, *Adv. Phys.* **23**, 1 (1974).
3. T. Ishihara, J. Takahashi, T. Goto, *Phys. Rev. B* **42**, 11099 (1990).
4. J. Calabrese *et al.*, *J. Am. Chem. Soc.* **113**, 2328 (1991).
5. M. F. Mostafa, M. M. Abdel-Kader, S. S. Arafat, E. M. Kandeel, *Phys. Scr.* **43**, 627 (1991).
6. H. Arend, K. Tichy, K. Baberschke, F. Rys, *Solid State Commun.* **18**, 999 (1976).
7. P. Day and R. D. Ledsham, *Mol. Cryst. Liq. Cryst.* **86**, 163 (1982).
8. B. Tieke and G. Chapuis, *ibid.* **137**, 101 (1986).
9. G. F. Needham, R. D. Willett, H. F. Franzen, *J. Phys. Chem.* **88**, 674 (1984).
10. D. B. Mitzi, C. A. Feild, W. T. A. Harrison, A. M. Guloy, *Nature* **369**, 467 (1994).
11. G. C. Papavassiliou, I. B. Koutselas, A. Terzis, M.-H. Whangbo, *Solid State Commun.* **91**, 695 (1994).
12. R. A. Mohan Ram, P. Ganguly, C. N. R. Rao, *J. Solid State Chem.* **70**, 82 (1987).
13. R. A. Mohan Ram, L. Ganapathi, P. Ganguly, C. N. R. Rao, *ibid.* **63**, 139 (1986).
14. R. J. Cava *et al.*, *Phys. Rev. B* **46**, 14101 (1992).
15. For $m = 2$, $CH_3NH_2{\cdot}HI$ (2.772 g, 17.44 mmol), NH_2CN (0.733 g, 17.44 mmol), and SnI_2 (6.495 g, 17.44 mmol) were dissolved in 70 ml of 57 weight % aqueous HI solution at 80°C. After soaking at 80°C for 12 hours, the solution was cooled to −10°C at 2°C/hour. The product was filtered under nitrogen, dried in flowing argon at 80°C for several hours, and then removed to an argon-filled dry box with oxygen and water levels maintained at <1 part per million. Powder x-ray diffraction indicated that the product was free of secondary phases such as starting materials, $CH_3NH_3SnI_3$, and higher m members of the homologous series. Crystals of the $m = 3$ compound were grown with a similar technique but with a 2:5:5 molar ratio of NH_2CN, $CH_3NH_2{\cdot}HI$, and SnI_2. The product contained a mixture of $m = 3$ and $CH_3NH_3SnI_3$. The sheet-like $m = 3$ crystals could be mechanically separated from the rod-like or rhombic dodecahedral cubic perovskite crystals because of the very different crystalline habit for these two materials. Isolated single crystals of $m = 4$ were similarly extracted from samples prepared in a solution containing a large excess of $CH_3NH_2{\cdot}HI$ and SnI_2.
16. E. N. Zil'berman, *Russ. Chem. Rev.* **31**, 615 (1962).
17. M. L. Kilpatrick, *J. Am. Chem. Soc.* **69**, 40 (1947).
18. D. Lin-Vien, N. B. Colthup, W. G. Fateley, J. G. Grasselli, Eds., *Handbook of Infrared and Raman Characteristic Frequencies of Organic Molecules* (Academic Press, New York, 1991).
19. T. N. Sumarokova, R. A. Slavinskaya, I. G. Litvyak, Z. F. Orlova, *Russ. J. Inorg. Chem.* **13**, 561 (1968).
20. L. J. Bellamy, *Infrared Spectra of Complex Molecules*, vol. 1 (Chapman and Hall, New York, 1986).
21. M. Nanot, F. Queyroux, J.-C. Gilles, A. Carpy, J. Galy, *J. Solid State Chem.* **11**, 272 (1974).
22. E. T. Keve, S. C. Abrahams, J. L. Bernstein, *J. Chem. Phys.* **53**, 3279 (1970).
23. J. D. Donaldson and S. M. Grimes, *Rev. Silicon Germanium Tin Lead Compd.* **8**, 1 (1984).
24. D. B. Mitzi, C. A. Feild, Z. Schlesinger, R. B. Laibowitz, *J. Solid State Chem.* **114**, 159 (1995).
25. J. Takada, H. Awaji, M. Koshioka, A. Nakajima, W. A. Nevin, *Appl. Phys. Lett.* **61**, 2184 (1992).
26. D. B. Mitzi, unpublished material.

27. We thank T. Jackman, B. A. Scott, and A. Jacobson for stimulating discussions, and M. Ritter for use of a displex system for measuring the resistivity of these samples.

28 October 1994; accepted 9 January 1995

A "Double-Diamond Superlattice" Built Up of $Cd_{17}S_4(SCH_2CH_2OH)_{26}$ Clusters

T. Vossmeyer, G. Reck, L. Katsikas, E. T. K. Haupt, B. Schulz, H. Weller*

A simple preparation of $Cd_{17}S_4(SCH_2CH_2OH)_{26}$ clusters in aqueous solution leads to the formation of colorless blocky crystals. X-ray structure determinations revealed a superlattice framework built up of covalently linked clusters. This superlattice is best described as two enlarged and interlaced diamond or zinc blende lattices. Because both the superlattice and the clusters display the same structural features, the crystal structure resembles the self-similarities known from fractal geometry. The optical spectrum of the cluster solution displays a sharp transition around 290 nanometers with a large absorption coefficient (~84,000 per molar per centimeter).

In the nanometer-size regime, the optical and transport properties of semiconductor clusters are controlled by the cluster size, whereas their chemical composition remains almost unchanged (*1*–*6*). For example, the optical properties of CdS nanoclusters change enormously with decreasing cluster size: The onset of absorption is shifted to higher energies, and the volume-normalized oscillator strength of the lowest electronic (excitonic) transition increases dramatically (*7*). These size effects result from the spatial confinement of the photogenerated charge carriers to the dimensions of the cluster, which can be represented by the quantum mechanical model of a "particle in a box" (*8*). One of the most exciting questions is how solid-state properties develop when regular macroscopic structures are built up by the packing of clusters into a three-dimensional framework, as is fulfilled in crystallized cluster samples.

Because of cluster-cluster interactions, interesting collective phenomena are to be expected, and such well-structured systems should be useful for learning how quantum-size effects can be used for electronic devices. So far, only van der Waals or ionic crystals built up of CdS clusters, such as $Cd_{32}S_{14}(SC_6H_5)_{36} \cdot 4$ DMF (*1*)